1-1-2018

Fatigue and Crack-Growth Behavior in a Titanium Alloy under Constant-Amplitude and Spectrum Loading

Kalyan Raj Kota

Fatigue and crack-growth behavior in a titanium alloy under constant-amplitude and spectrum loading

By

Kalyan Raj Kota

A Thesis
Submitted to the Faculty of
Mississippi State University
in Partial Fulfillment of the Requirements
for the Degree of Master of Science
in Aerospace Engineering
in the Department of Aerospace Engineering

Mississippi State, Mississippi

May 2018

Fatigue and crack-growth behavior in a titanium alloy under constant-amplitude and spectrum loading

By

Kalyan Raj Kota

Approved:

James C. Newman Jr.
(Major Professor)

Thomas E. Lacy
(Co-Major Professor)

Shantia Yarahmadian
(Committee Member)

Ratneshwar Jha
(Graduate Coordinator)

Jason M. Keith
Dean
Bagley College of Engineering

Name: Kalyan Raj Kota

Date of Degree: May 4, 2018

Institution: Mississippi State University

Major Field: Aerospace Engineering

Major Professors: Dr. James C. Newman Jr. and Dr. Thomas E. Lacy Jr.

Title of Study: Fatigue and crack-growth behavior in a titanium alloy under constant-amplitude and spectrum loading

Pages in Study 38

Candidate for Degree of Master of Science

A titanium alloy plate material was provided by the University of Dayton Research Institute. Fatigue-crack-growth tests on compact specimens have been previously performed at Mississippi State University. These tests used newly-developed compression pre-cracking method to generate fatigue-crack-growth-rate data in the near-threshold regime. A crack-closure model was then used to determine an effective stress-intensity-factor-range relation over a wide range in rates and load ratios ($R=P_{min}/P_{max}$). Some engineering estimates were made for extremely slow rates, below the commonly defined threshold rate. Single-edge-notch-bend fatigue specimens were machined from the titanium alloy plates and were tested at two load ratios (R = 0.1 and 0.5) and a modified Cold-Turbistan engine spectrum. Calculated fatigue lives from FASTRAN using small-crack theory with an equivalent-initial-flaw-size of 9 μm in radius at the center of the semi-circular edge notch fit the constant-amplitude test data fairly well, but underpredicted the spectrum loading results by about a factor of 2 to 3.

DEDICATION

Every challenging work needs self-efforts as well as support of elders especially those who were very close to our heart. I dedicate my humble effort to my sweet and loving

Amma & Nanna

whose affection, love, encouragement, and blessings made me achieve this success.

ACKNOWLEDGEMENTS

Immeasurable appreciation and deepest gratitude for the help and support extended to the following persons who in one way or another contributed in making this study possible.

Dr. James C. Newman Jr., for his support and guidance throughout this research. It has been an honor to work with him. And I am obliged for the opportunity of this inspiring road to the accomplishment of this thesis and I know it would have not been possible without him.

Dr. Thomas E. Lacy Jr., for his valuable suggestions and comments that proved valuable to this thesis along with the support, care, and words of encouragement in doing this research.

Dr. Shantia Yarahmadian, for his time and effort in checking this manuscript, and for serving on my committee.

To my family, friends, and colleagues, for their constant support and encouragement.

TABLE OF CONTENTS

LIST OF TABLES

LIST OF FIGURES

NOMENCLATURE

a	crack depth in thickness direction, mm
a_i	initial crack depth in thickness direction, mm
B	specimen thickness, mm
c	crack length in width direction, mm
c_i	initial crack length in width direction, mm
D	edge-notch diameter, mm
da/dN	crack-growth rate in depth direction, m/cycle
dc/dN	crack-growth rate in width direction, m/cycle
E	modulus of elasticity, MPa
f	loading frequency, Hz
K	stress-intensity factor, MPa√m
K_{Ie}	elastic fracture toughness, MPa√m
K_{max}	maximum stress-intensity factor, MPa√m
K_T	elastic stress-concentration factor
N	number of cycles
N_f	number of cycles to failure
P	applied load, kips
P_{max}	maximum applied load, kN
P_{min}	minimum applied load, kN

P_o	crack-opening load, kN
R	load ratio (P_{min}/P_{max})
r	edge-notch radius, mm
S	applied remote stress, MPa
S_{max}	maximum applied stress, MPa
S_{min}	minimum applied stress, MPa
So	crack-opening stress, MPa
W	specimen width, mm
α	tensile constraint factor
β	compressive constraint factor
ΔK	stress-intensity factor range, MPa$\sqrt{m}$
ΔK_{eff}	effective stress-intensity factor range, MPa$\sqrt{m}$
ρ	plastic-zone size, mm
σ_o	flow stress (average of σ_{ys} and σ_u), MPa
σ_{ys}	yield stress (0.2 percent offset), MPa
σ_u	ultimate tensile strength, MPa
ω	cyclic plastic-zone size, mm

Abbreviations

ASTM	American Society for Testing and Materials
CPCA	Compression precracking constant amplitude
CPLR	Compression precracking load-reduction
C(T)	Compact (tension) specimen

EIFS	Equivalent-initial-flaw-size
FTA	Fatigue Technology Associates
HCF	High-Cycle-Fatigue
LCD	Linear-cumulative damage
MSU	Mississippi State University
SEM	Scanning electron microscopy
SEN(B)	Single-edge-notch (bend) specimen
SEN(T)	single-edge-notch (tension) specimen
STOA	Solution treated and over-aged
UDRI	University of Dayton Research Institute

CHAPTER I

INTRODUCTION

1.1. Introduction

Titanium alloys are extensively used in manufacturing airframe, high-cycle propeller, and engine components. They have relatively high strength to weight ratio, extraordinary corrosion resistance, and acceptable performance at extremely high temperatures (750°F) [1-3]. The primary goal of this study is to improve the understanding of fatigue crack growth rate behavior of a titanium alloy in the threshold and near-threshold regimes. In United States, the fatigue-crack-growth threshold is defined using the American Society for Testing and Materials (ASTM) standard E-647 [4], which has exhibited irregularities such as "fanning" (larger spread among the crack-growth-rate curves with load ratio, R, in the threshold region than in the mid-region) due to the load-shedding test procedure for some materials. The fanning behavior in the threshold region of da/dN is assumed to be caused by an increase in the crack closure in the low R tests. Newman *et al.* have conducted tests and analyses on aluminum alloys, titanium alloys, and steels; and they have developed new threshold test methods – compression precracking constant-amplitude (CPCA) and compression precracking load-reduction (CPLR) [5-7].

A titanium alloy that was solution treated and over-aged (Ti-6Al-4V STOA) plate material was provided by the University of Dayton Research Institute (UDRI) from a

previous United States Air Force high-cycle fatigue study [8]. The scope of this research project [9] was to test a titanium alloy plate material provided by UDRI to: (1) conduct fatigue tests on single-edge-notch-bend, SEN(B), specimens at two constant-amplitude stress ratios (R = 0.1 and 0.5) and an engine spectrum (a modified Cold-Turbistan) loading, (2) develop the closure-based effective stress-intensity factor range against rate curve from compact specimen data on the same material, and (3) determine an equivalent-initial-flaw-size (EIFS) to fit the fatigue test data. All of the tests were conducted under laboratory air and room temperature.

Fatigue tests were conducted on single-edge-notch-bend, SEN(B), specimens at two constant-amplitude load ratios (R = 0.1 and 0.5) and modified Cold-Turbistan engine spectrum. The fatigue-life-prediction code, FASTRAN [10], was used to calculate the fatigue lives using small-crack theory with an equivalent-initial-flaw-size (semi-circular flaw) of 9 μm in radius at the center of the semi-circular edge notch fit the constant-amplitude test data very well, but underpredicted the spectrum loading results by about a factor of 2 to 3. Life predictions made with linear-cumulative damage (LCD) calculations agreed fairly well with the spectrum tests.

1.2. References

[1] Sha W. and Malinov S. (2009) Titanium Alloys: Modelling of Microstructure, Properties and Applications. *Elsevier*.

[2] Donachie M. J. (2000) Titanium Alloys: A Technical Guide. 2nd ed. *ASM International*.

[3] Joshi V. A. (2006) Titanium Alloys: An Atlas of Structures and Fracture Features. CRC Press.

[4] Standard Test Method for Measurement of Fatigue Crack Growth Rates (2012) *ASTM E-647*, West Conshohocken, PA.

[5] Newman, J. C., Jr., Schneider, J., Daniel, A. and McKnight, D. (2005) Compression Pre-cracking to Generate Near Threshold Fatigue-Crack-Growth Rates in Two Aluminum Alloys. *International Journal of Fatigue*, 27, 1432-1440.

[6] Newman, J.C., Jr. and Yamada, Y. (2010) Compression Precracking Methods to Generate Near-Threshold Fatigue-Crack-Growth-Rate Data. *International Journal of Fatigue*, 32, 879-885.

[7] Ruschau, J. J., and Newman, J. C., Jr. (2008) Compression Precracking to Generate Near Threshold Fatigue-Crack-Growth Rates in an Aluminum and Titanium Alloy, *ASTM International*, 5(7), pp. 1–11.

[8] Gallagher, J. P. (2001) Improved High-Cycle Fatigue (HCF) Life Prediction. AFRL-ML-WP-TR-2001-4159.

[9] Newman, J. C., Jr., Kota, K., and Lacy. T. E. (2017) Fatigue and crack-growth behavior in a titanium alloy under constant-amplitude and spectrum loading. *Engineering Fracture Mechanics*.

[10] Newman, J. C., Jr. (2013) FASTRAN—A Fatigue Crack Growth Life Prediction Code Based on the Crack-Closure Concept. Version 5.4 User Guide. Fatigue and Fracture Associates, LLC, Eupora, MS.

CHAPTER II

FATIGUE AND CRACK-GROWTH BEHAVIOR IN A TITANIUM ALLOY UNDER CONSTANT-AMPLITUDE AND SPECTRUM LOADING

2.1. Abstract

A titanium alloy (Ti-6Al-4V STOA) plate material was provided by the University of Dayton Research Institute from a previous U.S. Air Force high-cycle fatigue study. Fatigue-crack-growth tests on compact, C(T), specimens have been previously performed at Mississippi State University on the same material over a wide range in rates from threshold to near fracture for several load ratios ($R = P_{min}/P_{max}$). These tests used the compression pre-cracking method to generate fatigue-crack-growth-rate data in the near-threshold regime. Current load-reduction procedures were found to give elevated thresholds compared to compression pre-cracking methods. A crack-closure model was then used to determine crack-front constraint and a plasticity-corrected effective stress-intensity-factor-range relation over a wide range in rates and load ratios. Some engineering estimates were made for extremely slow rates (small-crack behavior), below the commonly defined threshold rate. Single-edge-notch-bend, SEN(B), fatigue specimens were machined from titanium alloy plates and were fatigue tested at two constant-amplitude load ratios (R = 0.1 and 0.5) and a modified Cold-Turbistan engine spectrum. Calculated fatigue lives from FASTRAN, a fatigue-life-prediction code, using small-crack theory with an equivalent-initial-flaw-size (semi-circular surface flaw) of

9 μm in radius at the center of the semi-circular edge notch fit the constant-amplitude test data fairly well, but underpredicted the spectrum loading results by about a factor of 2 to 3. Life predictions made with linear-cumulative damage (LCD) calculations agreed fairly well with the spectrum tests.

2.2. Introduction

In 1961, the classic paper by Paris, Gomez and Anderson [1] on "A Rational Analytical Theory of Fatigue" was a major development in the study of fatigue, see Figure 2.1. The newly emerging field of Fracture Mechanics, driven by the works of Griffith [2] and Irwin [3], began to help engineers characterize fracture of brittle materials; and to provide a crack-tip parameter, the stress-intensity factor (K), to correlate fatigue-crack-growth-rate data on metallic materials for different crack configurations, and provided a methodology to predict the failure of cracked structural components.

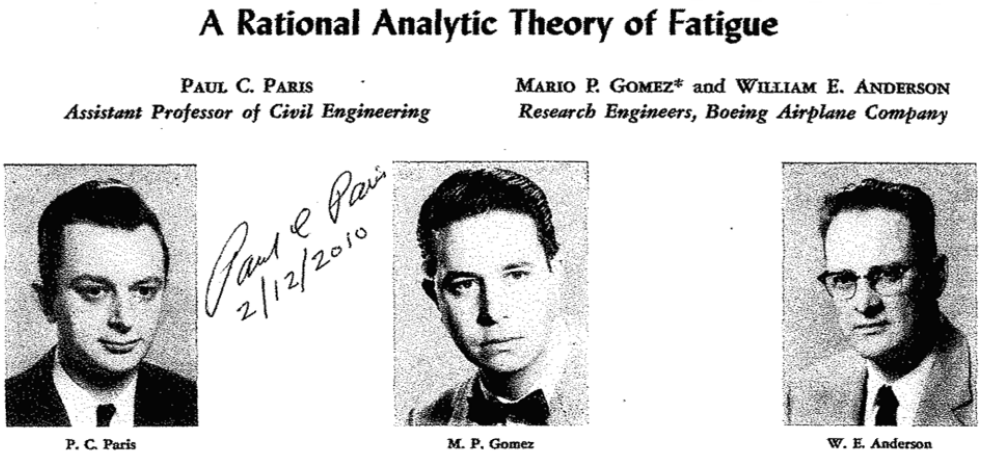
A Rational Analytic Theory of Fatigue

PAUL C. PARIS
Assistant Professor of Civil Engineering

MARIO P. GOMEZ* and WILLIAM E. ANDERSON
Research Engineers, Boeing Airplane Company

Paul C Paris 2/12/2010

P. C. Paris M. P. Gomez W. E. Anderson

Figure 2.1 Classic paper by Paris, Gomez and Anderson in *The Trends in Engineering* [1].

"Wild Bill" Anderson, as he was called, was very instrumental, at Boeing Airplane Company and, later, at the National Aeronautics and Space Administration Langley Research Center, in promoting these new concepts to the next generation. Several things were to be developed before "fatigue" could be predicted using Fracture Mechanics: (1) Stress-intensity factors for small surface cracks [4-6], (2) Crack-closure theory [7-9], (3) Plasticity effects on crack-driving parameters [10, 11], (4) Constraint effects on crack growth and closure [12, 13] and (5) Small- and large-crack data in the "threshold" regime without load-history affects [14-16]. After several decades of research, these concepts began to merge together and the vision that Paris and Anderson had in 1961 could now be achieved on "engineered" materials. Materials that nucleated cracks at constituent particles, inclusions, grain boundaries, voids, and, also, manufacturing defects. Newman proposed in developing the fatigue life prediction methods to predict micro-crack growth, as influenced by microstructure and environment, under complex load histories [17].

The current paper is another demonstration of using the principles of Fracture Mechanics to predict the fatigue behavior of notched specimens made of a titanium alloy. Fatigue-crack-growth-rate behavior in the threshold and near-threshold regimes is very important for the growth of small cracks for high-cycle propeller and engine components. However, the test procedures, which have been used to generate fatigue-crack-growth-rate data from laboratory specimens (American Society for Testing and Materials (ASTM) E-647 [18, 19]) in the past, have produced "fanning" with the load ratio (R) in the low-rate regime, using bend-type specimens. (Fanning of the ΔK_{th} thresholds as a function of R is the phenomenon where the spread among the crack-growth-rate curves

with R is significantly greater in the threshold region than in the mid-region.) During the past decade, it has been shown that data generated with the standard load-reduction test procedure exhibits configuration differences (results from tension and bend-type specimens differ), size effects (smaller specimens have produced lower thresholds and faster crack-growth rates than larger width specimens), and that environment plays a very important role in threshold development, as expected. Research work at Mississippi State University (MSU) on aluminum alloys, titanium alloys and steels have developed new threshold test methods – compression precracking constant-amplitude (CPCA) and compression precracking load-reduction (CPLR) threshold testing [15-16]. Efforts are underway to incorporate these new threshold testing methods into ASTM E-647 [18].

The scope of this research project was to test a titanium alloy plate material provided by University of Dayton Research Institute (UDRI) to: (1) conduct fatigue tests on single-edge-notch-bend, SEN(B), specimens at two constant-amplitude stress ratios (R = 0.1 and 0.5) and an engine spectrum (a modified Cold-Turbistan) loading, (2) develop the closure-based effective stress-intensity factor range against rate curve from compact specimen data on the same material, and (3) determine an equivalent-initial-flaw-size (EIFS) to fit the fatigue test data. All of the tests were conducted under laboratory air and room temperature.

2.3. Material

The titanium alloy material considered herein was a remnant from a United States Air Force High-Cycle-Fatigue (HCF) program [20], that was in the solution treated and over-aged (STOA) condition and produced in accordance with AMS 4928. The alpha–beta titanium alloy used in the HCF program had been processed in a way to minimize

residual stresses, but the slitting method was used to measure the residual stress-intensity factors on two 51 mm wide C(T) specimens [21]. These tests verified that the material did not have any significant residual stresses. The heat-treatment and aging process resulted in a microstructure with an average grain size of about 20 μm. The yield stress (σ_{ys}) was 931 MPa, the ultimate tensile strength (σ_u) was 979 MPa, and the modulus of elasticity (E) was 116 GPa.

2.4. Test Specimens

The material received from UDRI was in the form of plates roughly 20 x 115 x 415 mm. The plates were split and 6.35 mm thick SEN(B) specimens were machined, such that the cracks would nucleate and propagate in the same direction, as previously done on 6.35 mm thick C(T) specimens [22], as shown in Figure 2.2(a). The crack-mouth-opening-displacement gage was used to monitor crack growth; and the backface strain gage was used to measure residual stress-intensity factors [21].

A fatigue and small-crack test specimen had previously been designed in a U.S. Federal Aviation Administration contract with MSU [23]. The new specimen design was based on the AGARD small-crack (single-edge-notch tension, SEN(T)) specimen [24], and the configuration is shown in Figure 2.2(b). Although the specimen is subjected to tension, the notch-root test section is subjected to primarily bending with a small amount of tension contributing to the notch-root stress concentration. The notch-root stress σ_{max} is equal to 13.8 times the nominal stress, P/(WB). The thickness (B) was 6.35 mm, specimen width, W, was 25.4 mm, and the semi-circular notch diameter (D) was 6.35 mm. The notch root was mechanically polished to minimize machining residual stresses. Standard fatigue tests were conducted to generate the stress-life (S-N) data for

constant-amplitude and a modified engine disc spectrum (Cold Turbistan [25]) loading. The characteristic stress was given as P_{max}/ (WB), where P_{max} was the maximum load in the constant-amplitude or spectrum tests.

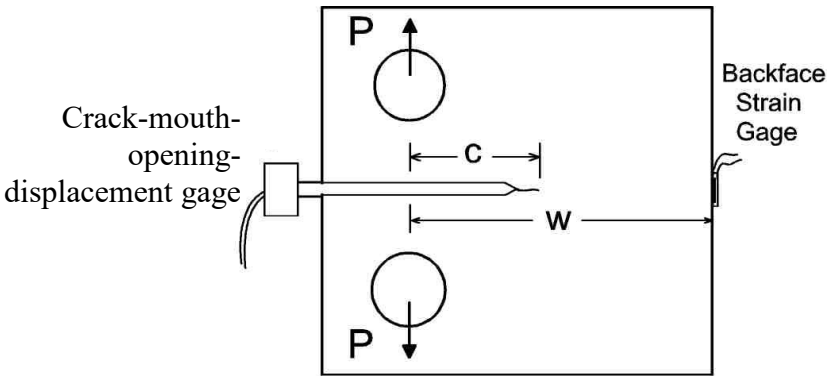

(a) Compact, C(T), specimen

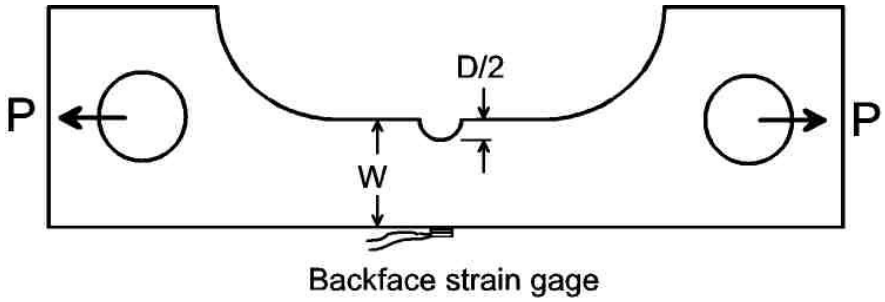

(b) Single-edge-notch-bend, SEN(B), specimen.

Figure 2.2 Crack growth and fatigue specimens tested and analyzed.

In the SEN(B) specimens, crack(s) should normally nucleate as surface cracks along the mid-section of the notch root (region of the highest stress concentration), but sometimes the nucleating site may be a corner crack. To help prevent an induced out-of-plane bending moment from the pin loading, the holes in the specimens were beveled using a circular file over about a ±20 deg. region on the pin-contacting side (about 1/3 of

the thickness on both sides, leaving a 1/3-of-thickness flat region for pin contact in the center of the specimen). (Beveling or counter-boring pin holes in C(T) specimens are currently being added to ASTM E-647, as an option to prevent non-straight crack fronts.) The backface strain gage, as shown in Figure 2(b), was used to monitor cracking damage along the notch root and to determine an approximate size of the crack emanating from the notch [23].

2.5. Test Loading Conditions and Procedures

2.2.1. Constant-Amplitude Loading

Fatigue (S-N) tests on SEN(B) specimens were conducted at R = 0.1 and 0.5 loading. The objective was to generate fatigue test data in the endurance limit region. Trial-and-error procedures were used to select the test load levels. For tests that reached or exceeded 10^7 cycles, the specimens were re-tested at a higher load level.

2.2.2. Spectrum Loading

Fatigue tests were also conducted on the SEN(B) specimens using an engine disc spectrum loading. A modification of a standard engine spectrum, Cold Turbistan [25], was selected. The Turbistan spectra are European standard engine spectra for hot or cold engines with various amounts of small amplitude omissions. The Cold Turbistan (10% omission) spectrum was selected but modified to have only tension-tension loads on the pin-loaded specimens. Thus, a mean load was added to all loads such that the overall load ratio (R) was 0.1. The spectrum had 3,149 cycles and was repeated until failure. The first part of the Cold Turbistan+ (10% omission) spectrum is shown in Figure 2.3. The loads have been normalized by the maximum load in the spectrum; and the spectrum is a

mixture of low and high R cyclic loading. The minimum load in the spectrum is 0.1 times the maximum load.

To help ensure accurate application of the spectrum loads, two training SEN(B) specimens (titanium alloy with same dimensions) were used to tune the test machines and to develop correction files that were then used with the Fatigue Technology Associates (FTA), LLC spectrum loading and crack monitoring system [26]. For a given maximum load, maximum load rate (30 kN/sec) and maximum frequency (10 Hz), a large number of spectrum repeats (8 to 16) were applied to train the software. During testing of the actual specimens, the appropriate correction file was then used and loads were more accurately applied from the first to last application of the spectra. In addition, a spectrum validation file was also created for each test. The validation file gave the target loads and actual applied loads during the complete test. On several occasions, these files were analyzed to verify the loading accuracy. During a test, the FTA software also outputs a damage parameter (generally, 0.99) that verifies the accuracy of current load applications.

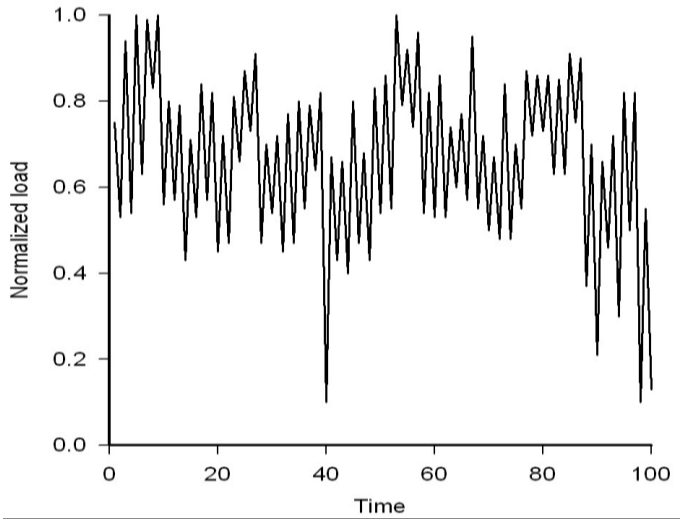

Figure 2.3 Part of the Cold-Turbistan+ engine spectrum.

2.6. Crack-Closure Modeling

The analytical crack-closure model was developed for a central crack in a finite-width plate subjected to uniform applied stress [9]. The model was based on the Dugdale model [27], but modified to leave plastically deformed material in the wake of the crack. The primary advantage of this model is that the plastic-zone size and crack-surface displacements are obtained by superposition of two elastic problems—a crack in a plate subjected to a remote uniform stress and a crack in a plate subjected to a uniform stress acting over a segment of the crack surface.

In the early 1980's, the analytical crack-closure model was extended to through cracks emanating from a circular hole in a finite-width plate also subjected to remote uniform applied stress [28]. This model was developed for analyzing one of the most important crack configurations in the aerospace industry—cracks at a fastener hole. The model is used for all cases of cracks emanating from a hole or notch using the K-analogy concept [29]. In developing the crack-from-a-hole model, some approximate equations were developed [28] to estimate the crack-surface displacements due to the remote applied stress and to the contact stress acting along the crack surface using the Tada, Paris and Irwin Stress-Intensity Factor Handbook [30].

Figure 2.4 shows a schematic of the model at maximum and minimum applied stress for a crack emanating from an open hole. The model is composed of three regions: (l) a linear-elastic region containing a fictitious crack of half-length $c^* + \rho$, (2) a plastic region of length ρ, and (3) a residual plastic deformation region along the crack surface. The length $c^* = r + c$, where the physical crack is of length c. The length of the compressive plastic zone is ω. Region 1 is treated as an elastic continuum. Regions 2 and

3 are composed of rigid-perfectly plastic (constant stress) bar elements with a flow stress, σ_o. The flow stress (σ_o) is the average between the yield stress and the ultimate strength of the material. This is a first order approximation for strain hardening. The shaded (dark) regions indicate material that is in a plastic state. At any applied stress level, the bar elements are either intact (in the plastic zone) or broken (residual plastic deformation). The broken elements can carry compressive loads only, and then only if they are in contact. At the maximum applied stress and when the crack is fully open, the effects of state of stress on plastic-zone size and displacements are approximately accounted for by using a constraint factor, α. The constraint factor is used to elevate the tensile flow stress for the intact elements in the plastic zone. The effective flow stress $\alpha\sigma_o$ for simulated plane-stress conditions is σ_o (usual Dugdale model) and for simulated plane-strain conditions is $3\sigma_o$. The value of $3\sigma_o$ was established from elastic-plastic finite-element analyses under plane-strain conditions using an elastic-perfectly-plastic material (normal stress elevation in the crack-tip region was about 2.7 from the analysis of a tension-loaded cracked specimen [13]). Irwin [10] suggested a modification to account for through-the-thickness variation in the stress state by introducing a constraint factor of $\alpha = 1.73$. This value of constraint represented nominal plane-strain conditions.

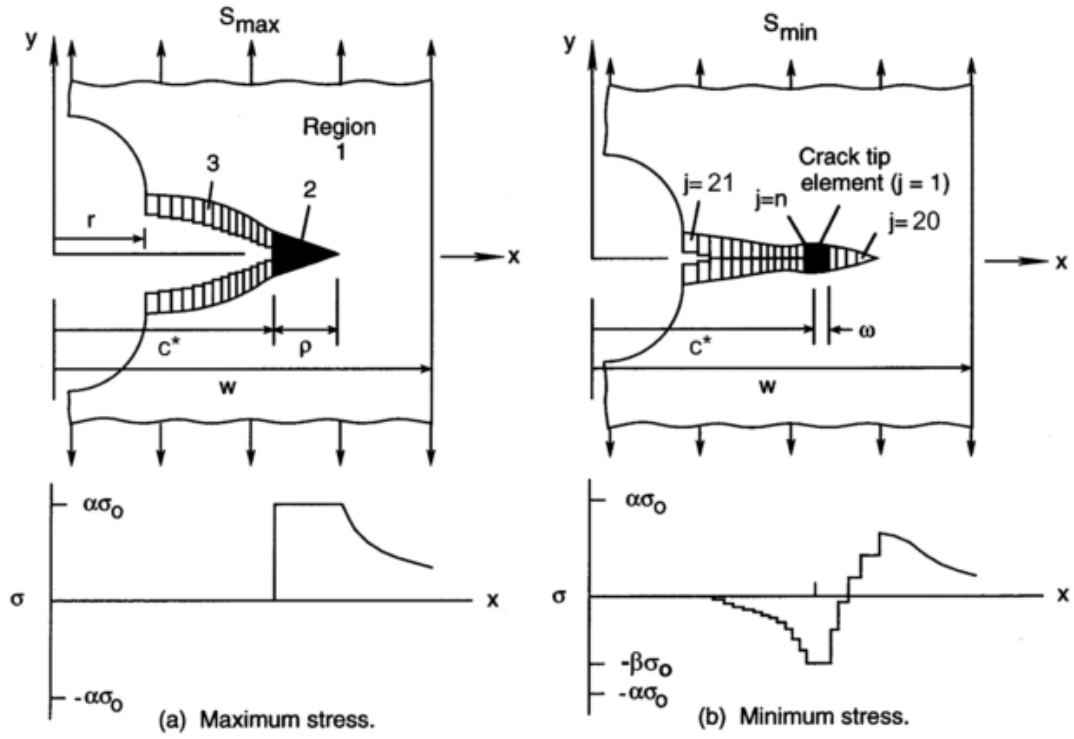

Figure 2.4 Schematic of analytical crack-closure model for a crack emanating from a circular hole under cyclic loading.

At the minimum applied stress, some elements in the plastic zone and elements along the crack surface that are in contact may yield in compression when the contact or compressive stress reaches $-\beta\sigma_o$. In the original model, the compressive constraint factor, β, was selected as unity. The loss of constraint under compression was justified on the grounds that when a crack closes the large stress gradient at the crack tip is greatly reduced and a more uniform stress field is produced. In addition, elements in the plastic zone and along the crack surface were assumed to have the same compressive constraint factor. More details on the model are given in Reference [31].

To improve the usefulness of the crack-closure model, a crack-opening-stress equation was developed [31, 32] that would give the crack-opening stress (S_o) as a function of the stress (load) ratio, R, applied stress level to flow stress ratio (S_{max}/σ_o), and the constraint factor (α). Since the large-crack data on C(T) specimens will be used to develop the effective stress-intensity-factor range against rate relation, a comparison is made between the crack-opening-stress equation and the FASTRAN model in Figure 2.5. Here the crack-opening-load ratio is plotted against the load ratio, R. The constraint factors were assumed to be $\alpha = 2$ and $\beta = 1$. The load level on C(T) specimens are very low, so S_{max}/σ_o was set to 0.1. For positive stress ratios, the stress level had a very weak effect on the crack-opening loads, but the stress level effect is very strong for negative stress ratios [31]. The symbols show the FASTRAN analyses with the load levels used in the C(T) tests (discussed later) at R = 0.1, 0.4 and 0.7. In the model, crack-opening loads stabilize under constant-amplitude loading after the crack has grown about a plastic-zone size. The largest difference in ΔK_{eff} between the equation (solid curve) and model would be about 2.5% for $R \leq 0.4$, but the crack was fully open ($\Delta K_{eff} = \Delta K$) at R = 0.7.

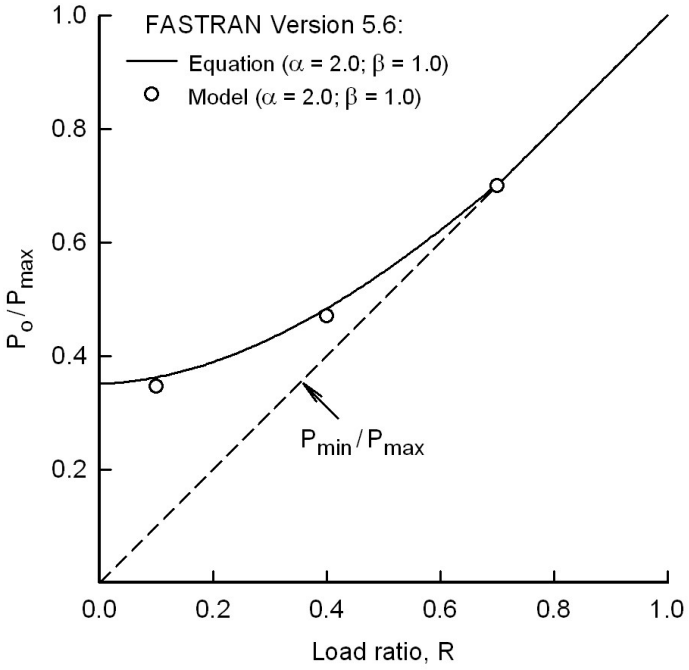

Figure 2.5 Crack-opening-load ratio from equation and FASTRAN model for nearly plane-strain conditions.

2.7. Large Crack Growth-Rate Behavior

To make life predictions, ΔK_{eff} as a function of the crack-growth rate must be obtained for the material and environment (lab air, temperature, etc.) of interest. Fatigue-crack-growth-rate data should be obtained over the widest possible range in rates (from threshold to fracture), especially if spectrum load predictions are required. Data obtained on the crack configuration of interest would be helpful, but it is not essential. Most damage-tolerant life calculations can be performed using linear elastic stress-intensity factor analysis with crack-closure modifications. In the following, the ΔK_{eff}-rate relation will be developed for the titanium alloy.

The linear-elastic effective stress-intensity factor range developed by Elber [8] is given by

$$\Delta K_{eff} = (S_{max} - S_o) \sqrt{(\pi c)}\, F(c/w) \tag{2.1}$$

where S_{max} is the maximum stress, S_o is the crack-opening stress, and F is the boundary-correction factor. (For the C(T) specimen, S = P/(WB) and F is modified accordingly [30].) However, for high stress-intensity factors, proof testing, and low-cycle fatigue conditions, the linear-elastic analyses are inadequate and nonlinear crack-growth parameters are needed. To account for plasticity, a portion of the cyclic-plastic-zone length (ω) has been added to the crack length, c. The cyclic-plastic-zone-corrected effective stress-intensity factor [11] is

$$(\Delta K_p)_{eff} = (S_{max} - S_o) \sqrt{(\pi d)}\, F(d/w) \tag{2.2}$$

where d = c + ω/4 and F is the cyclic plastic zone corrected boundary-correction factor. The cyclic plastic zone is given by

$$\omega = (1 - R_{eff})^2\, \rho/4 \tag{2.3}$$

where $R_{eff} = S_o/S_{max}$ and the plastic-zone size (ρ) for a crack in a large plate is

$$\rho = c\, \{\sec[\pi S_{max}/(2\alpha\sigma_o)] - 1\} \tag{2.4}$$

where α is a constraint factor [12] and σ_o is the flow stress. Herein, the cyclic plastic zone corrected effective stress-intensity factor range, which is related to the cyclic J-integral, will be used in the fatigue-life predictions.

The ΔK_{eff}-rate relations and the $\Delta K_{eff}/E$ against rate plot on a variety of materials *i.e.,* aluminum 2024-T3, 7075-T6, 7075-T6 forging, 7075-T7351 Forging, AerMet-100; 4340 Steel, C-250 Steel, and Ti-62222 is shown in Figure 2.6. The results show a remarkable collapsing of data over many orders-of-magnitude in rate. Of interest for this

study was the uniqueness in the threshold region. Thus, the solid vertical line shows that the effective stress-intensity-factor-range threshold normalized by the modulus of elasticity, $(\Delta K_{eff})_{th}/E$, was about 1.2e-05 $\sqrt{m}$.

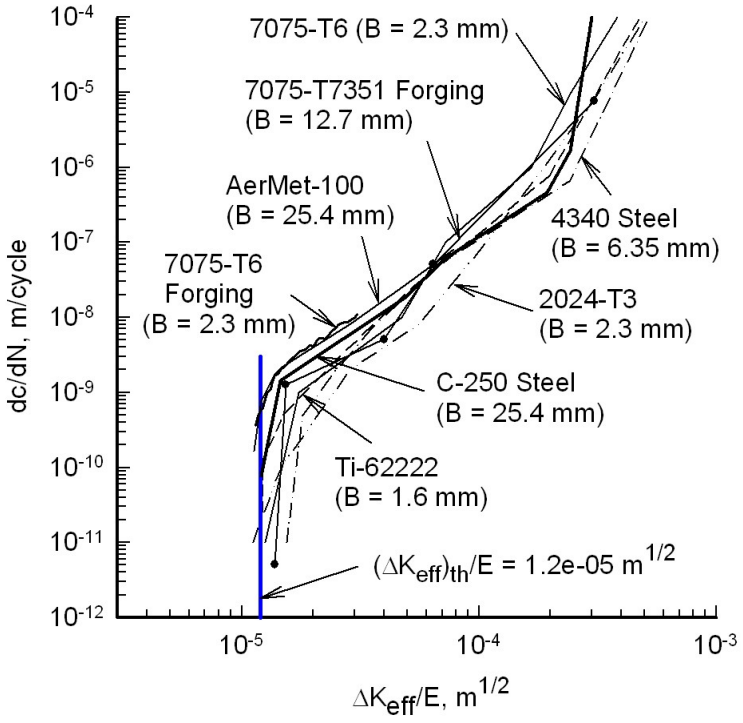

Figure 2.6 Normalized effective stress-intensity factor against rate for a variety of materials

Ruschau and Newman [22] tested C(T) specimens made of the titanium (Ti-6Al-4V STOA) alloy over a wide range in rates and load ratios (R = 0.1, 0.4 and 0.7) for a range in widths (W = 25, 51 and 76 mm). The reason for testing a wide range in C(T) widths was that Garr and Hresko [33] had previously found a width effect in determining ΔK_{th} values using the current ASTM E647 load-shedding method [18] on an Inconel-718 superalloy. For the titanium alloy, there was also a strong width effect on near-threshold

behavior using E647; but the newly developed compression pre-cracking constant-amplitude (CPCA) method did not show a width effect [21, 22].

Newman et al. [21] used these data to develop the ΔK_{eff}-rate relation, as shown in Figure 2.7. It was found that a constraint factor (α) of 2 correlated the data for the three R values very well. A constraint-loss regime occurs at the high rates, where $(\Delta K_{eff})_T = 0.5\ \sigma_o \sqrt{B}$ for tension-loaded cracked configurations [12], but further study is required for deep cracks in bend specimens, such as the C(T) specimen. As shown in Figure 2.7, test data did not go below the ASTM defined threshold rate (1.0e-10 m/cycle [18]). Thus, an extrapolation had to be made for extremely low crack-growth rates using the estimated $(\Delta K_{eff})_{th}$ value (shown by the vertical dashed line using the modulus of elasticity, as shown in Fig. 2.6).

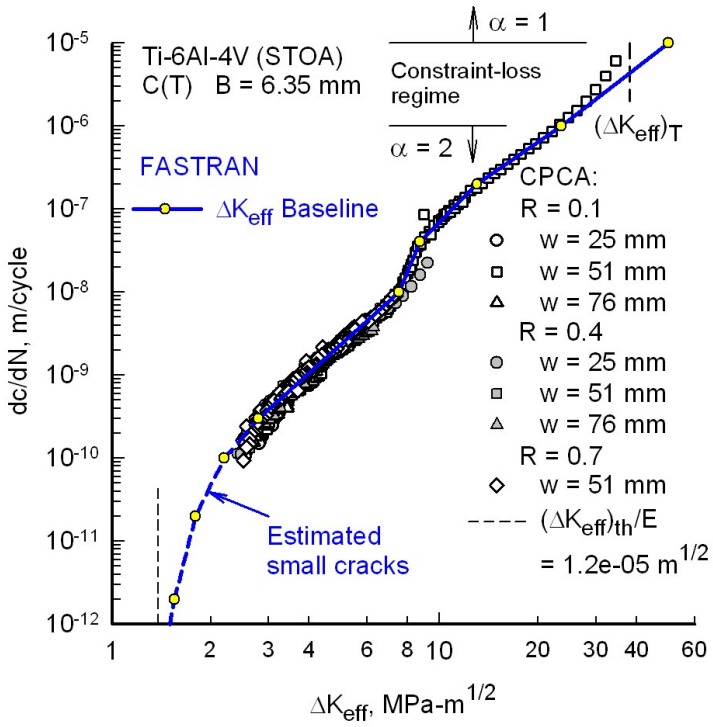

Figure 2.7 Effective stress-intensity factor against rate for Ti-6Al-4V (STOA) material.

Figure 2.8 shows the ΔK-rate data at R = 0.1 test conditions for the three C(T) specimen widths. The data correlated very well in the low-rate regime indicating that the stress-intensity-factor concept worked well using the CPCA method [15, 16]. As previously mentioned, the ASTM E647 load-shedding method produced a width effect in the near-threshold regime [22, 33]. The solid curve is the calculated results from the crack-closure model, which fit the test data very well. Further efforts are required to develop a test procedure to generate extremely low crack-growth rates below 1.0e-10 m/cycle. In this regime, crack growth is not on a cycle-by-cycle basis, but intermittent, where crack fronts may stop at grain boundaries or other microstructural features and take many cycles to re-initiate. Thus, these extremely slow rates are "average" values over many thousands of cycles. Therefore, new measurement procedures may have to be developed using the scanning-electron-microscope (SEM) on small surface- and corner-crack propagation patterns.

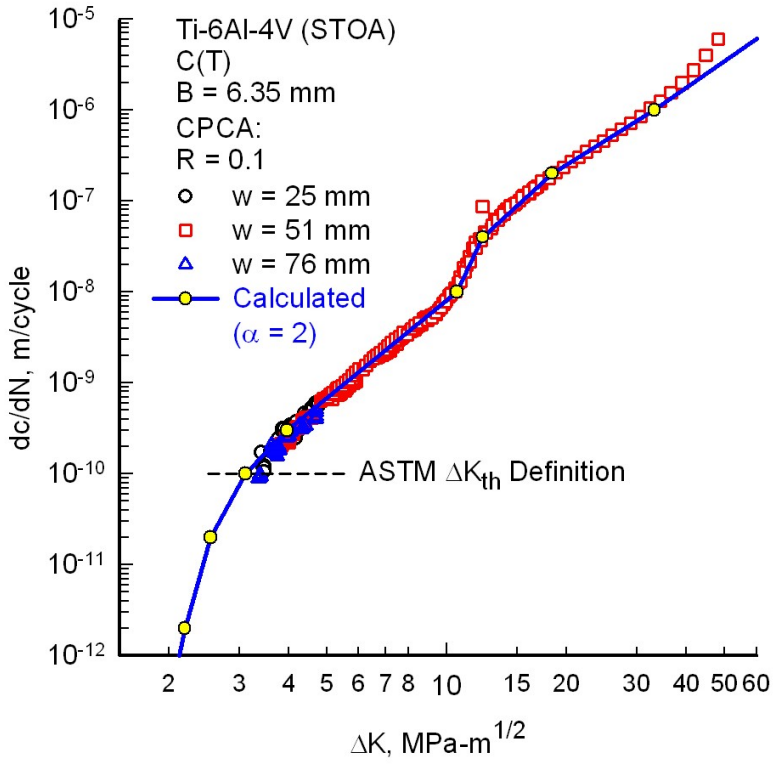

Figure 2.8 Linear-elastic stress-intensity-factor range against rate for Ti-6Al-4V (STOA).

2.8. Fatigue (S-N) Behavior Using Small-Crack Theory

In fatigue studies, it appears that the traditional "endurance" limits may not exist for engineered materials under very high-cycle fatigue (HCF) conditions. Conventional fatigue design codes still base their recommendations on the existence of endurance limits. But several investigations clearly show that in the HCF regime, a decrease of fatigue strength with increased number of cycles still occurs [34]. Thus, in using Small-Crack Theory to predict fatigue behavior of metallic materials, it also appears that fatigue-crack-growth thresholds, ΔK_{th}, may not exist [35].

The FASTRAN [31] life-prediction code was used to model crack growth from an initial micro-structural size flaw to failure and the crack-growth relation used is

$$dc/dN = C_{1i} (\Delta K_{eff})^{C_{2i}} [1 - (\Delta K_o/\Delta K_{eff})^p]/[1 - (K_{max}/K_{Ie})^q] \quad (2.5)$$

where C_{1i} and C_{2i} are the coefficient and exponent for each linear segment (i = 1 to n), respectively. ΔK_{eff} is the effective stress-intensity factor, ΔK_o is the effective threshold, K_{max} is the maximum stress-intensity factor, K_{Ie} is the elastic fracture toughness (which is, generally, a function of crack length, specimen width, and specimen type), p and q are constants selected to fit test data in either the threshold or fracture regimes, respectively. Herein, no threshold was modeled and ΔK_o was set equal to zero; thus, p was not needed. Near-threshold behavior was modeled with the multi-linear equation. Fracture was modeled using the Two-Parameter Fracture Criterion (K_F and m) [36]. (The elastic-plastic fracture toughness, $K_F = K_{Ie}/(1 - m\ S_n/\sigma_u)$, where m is a fracture ductility parameter. Thus, if m = 0, then $K_F = K_{Ie}$, and fracture is controlled by linear-elastic fracture mechanics.) However, in fatigue life predictions the fracture toughness is not very important because a two-fold change in the critical stress-intensity factor at failure would have an insignificant effect on fatigue life (less than a few percent). The tabular values of ΔK_{eff} against rate, fracture properties (K_F and m), and tensile properties (σ_{ys}, σ_u and E) are given in Table 2.1 for the Ti-6Al-4V (STOA) material. The flow stress, σ_o, used in the FASTRAN model was the average between yield stress and ultimate tensile strength.

Table 2.1 Effective stress-intensity-factor range against rate relation, fracture and tensile properties for Ti-6Al-4V (STOA) alloy.

ΔK_{eff}, MPa$\sqrt{m}$	da/dN, dc/dN, m/cycle
1.4	2.0e-13
1.55	2.0e-12
1.8	2.0e-11
2.2	1.0e-10
2.8	3.0e-10
7.5	1.0e-08
8.7	4.0e-08
13.0	2.0e-07
23.5	1.0e-06
50.0	1.0e-05
$\alpha_1 = 2$	$\leq$ 1.0e-06
$\alpha_2 = 1$	$\geq$ 1.0e-05
K_{Ie} = 66 MPa$\sqrt{m}$	m = 0
σ_{ys} = 931 MPa	σ_u = 979 MPa
E = 116 GPa	σ_o = 955 MPa

A surface crack at a notch configuration is shown in Figure 2.9(a). The surface crack was grown in both the a- and c-directions using a cycle-by-cycle calculation. The a-direction was measured at the location where the crack intersected the notch free surface and was in the thickness direction; while the c-direction was at the maximum depth location from the notch root and grew in the width direction. The rate in the a-direction (da/dN) was assumed to have the same ΔK_{eff}-rate relation as in the c-direction (dc/dN), as given in Table 2.1. When the crack depth, a, reached the plate half-thickness (a/t = 1), the surface crack abruptly became a through crack of length, c, from the notch, see Figure 2.9(b). To make fatigue-life calculations or predictions on SEN(B) specimens, an initial

semi-circular surface crack ($a_i = c_i$) was determined by trial-and-error to fit the constant-amplitude fatigue tests on the titanium alloy. The effective stress-intensity factor is

$$\Delta K_{eff} = [(P_{max} - P_o)/(WB)] \sqrt{(\pi c)}\, F \qquad (2.6)$$

where F(a/c, a/B, r/W, ϕ) is the boundary-correction factor for a surface crack or a through crack at the semi-circular notch [37]. The parametric angle, ϕ, is zero for the a-direction and $\phi = \pi/2$ for the c-direction. At $\phi = 0$ (crack intersection location with free notch surface), a β_R factor was applied to reduce ΔK to account for "plane-stress" behavior [37]. The crack-opening load, P_o, was calculated from FASTRAN [31] under constant- or variable-amplitude loading.

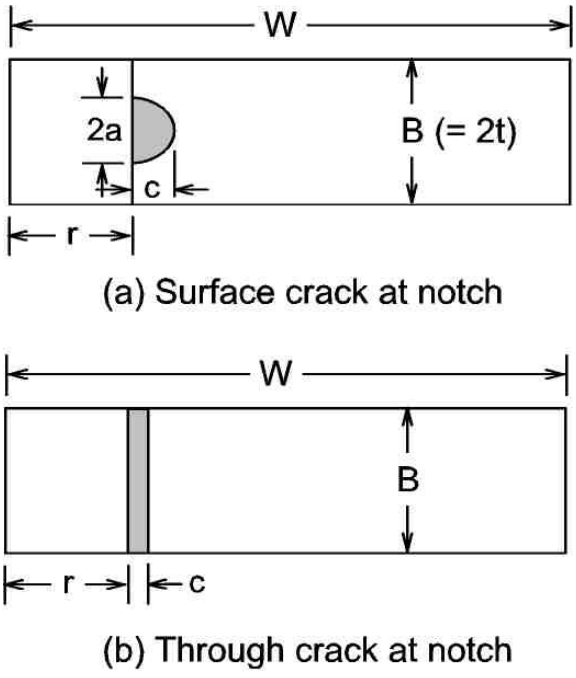

Figure 2.9 Surface- and through-crack at semi-circular edge notch in SEN(B) specimen.

Fatigue tests on the SEN(B) specimens were conducted under constant-amplitude loading at R = 0.1. These results are shown in Figure 2.10, as solid circular symbols. An arrow on a symbol indicates a runout or stopped specimen. Two specimens that had reached 1.0e+07 cycles (runout) were re-tested at a high load level (open circular symbols). It is apparent that the lower stress level applied to the runout specimens had damaged the material along the semi-circular notch and produced shorter fatigue lives than the other tests. All specimens failed with through-the-thickness cracks.

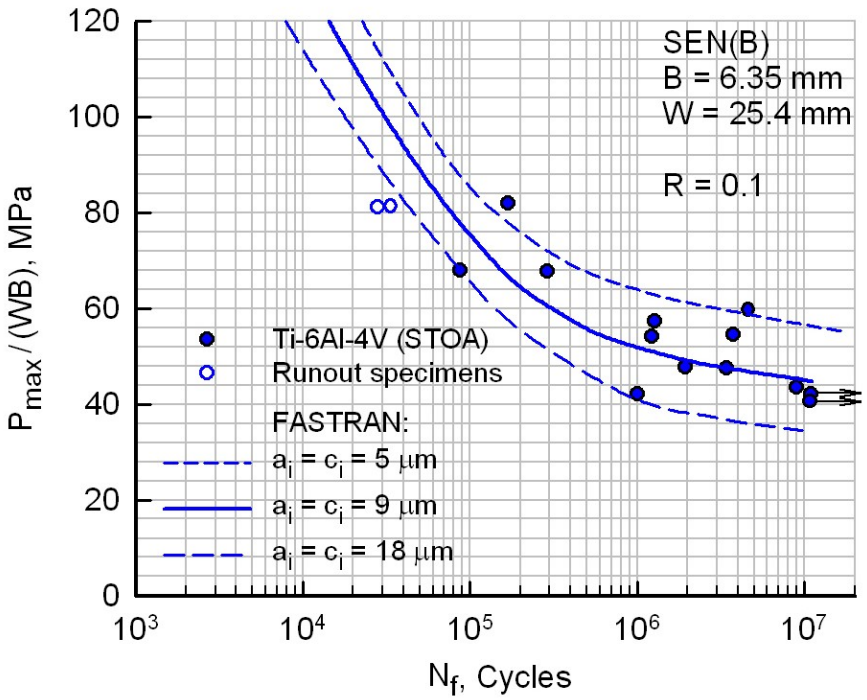

Figure 2.10 Fatigue life predictions from FASTRAN under R = 0.1 constant-amplitude loading.

The solid curve is a fatigue-life calculation from FASTRAN using a 9 μm initial semi-circular flaw size at the center of the semi-circular notch, using the ΔK_{eff}-rate curve from the STOA titanium alloy. The 9 μm flaw size is the equivalent-initial-flaw

size (EIFS) to fit the fatigue data. Crack-growth calculations were made in both the a- and c-directions for the surface crack, and a through crack when the crack depth reached the plate thickness. A 5 and 18 μm initial semi-circular flaw size produced very nice scatter bands.

An effort was made to determine the state of the semi-circular notch root after machining and polishing; and some possible metallurgical features that may have nucleated the fatigue failure (*cf.,* Fig. 2.11). In observing the fatigue surfaces with the naked eye, some dark features were found along the notch root that may have indicated the nucleation site(s). Both optical and scanning-electron-microscope (SEM) analyses were made to try to identify some of these features. The SEM analysis shows some features that look like the fatigue failures came from micro-machining marks and not the material micro-structure. The depth of the machining mark was about 7.4 μm, and the possible depth of the feature was about 14.8 μm. The EIFS of 9 μm was remarkably close to this micro-machining feature. It would appear that the 9 μm semi-circular flaw is a "real-initial-flaw size" and not an EIFS. But further study is needed.

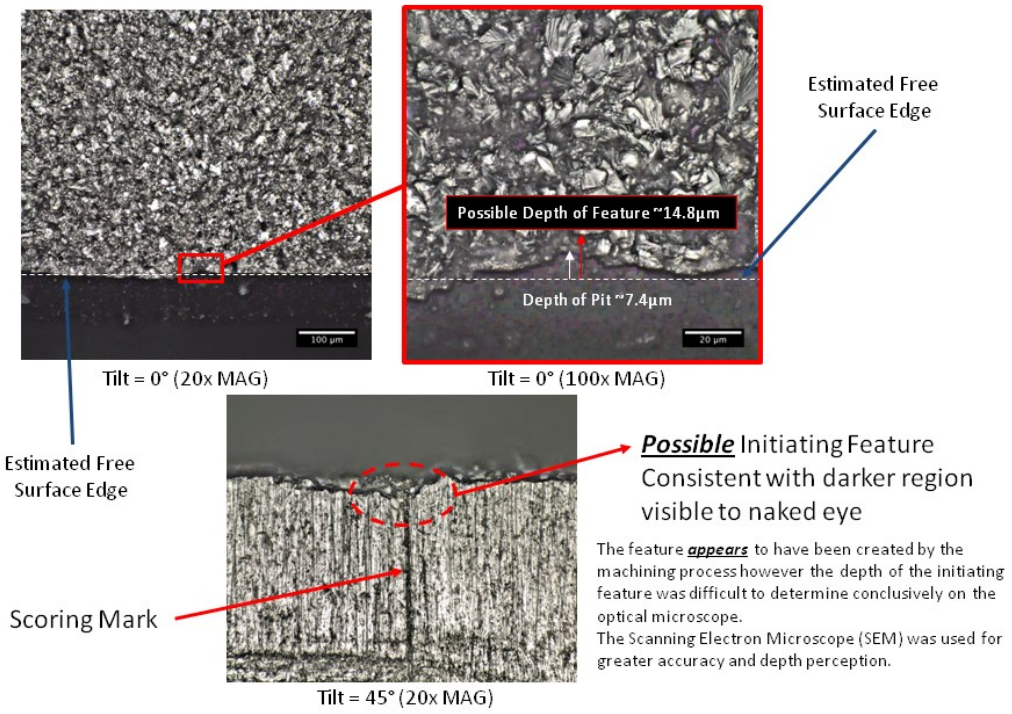

Figure 2.11 Scanning Electron Microscope photographs of one of the SEN(B) specimens.

Constant-amplitude fatigue tests at R = 0.5 on the SEN(B) specimens are shown in Figure 2.12, as closed symbols. Again, the predicted fatigue lives using FASTRAN with a 9 µm initial semi-circular flaw size at the center of the semi-circular notch agreed well with the test data. The single runout specimen was retested at a higher stress level, as shown by the open symbol. Again, it is apparent that the lower stress level initially applied to the runout specimen had damaged the material along the semi-circular notch root and produced a shorter fatigue life than predicted.

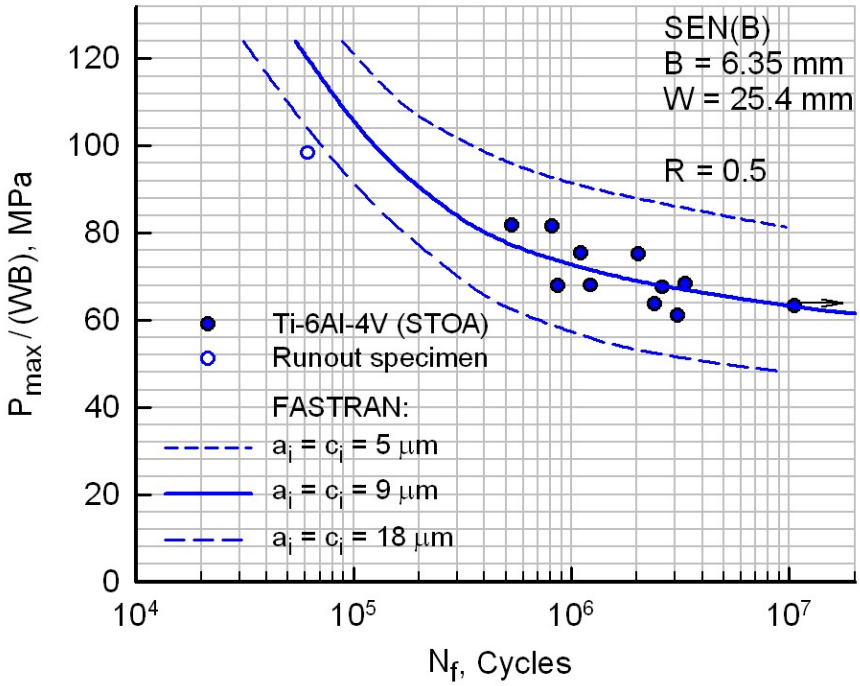

Figure 2.12 Fatigue life predictions from FASTRAN under R = 0.5 constant-amplitude loading.

Figure 2.13 shows the results on the Cold-Turbistan+ spectrum. For some reason, the FASTRAN fatigue-life predictions using the 9 μm initial flaw underpredicted the tests by a factor of two to three. Again, the dashed curves show the predicted results using either a 5 μm or an 18 μm semi-circular initial flaw size. The results from the 5 μm flaw agreed better with the test data. Thus, the FASTRAN input file for the Cold-Turbistan+ spectrum was checked for accuracy, especially, the conversion from the Fatigue Technology Associates (FTA) dat file to the FASTRAN input spectrum. In addition, the ΔK_{eff}-rate curve was studied again to see if there was some reason for the shorter predicted lives.

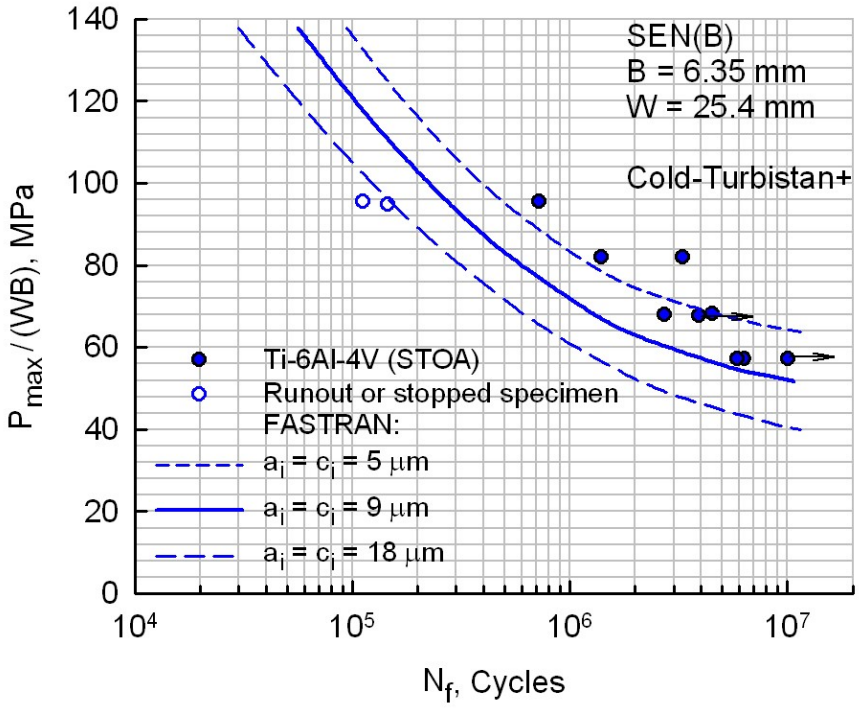

Figure 2.13 Fatigue life predictions from FASTRAN under Cold-Turbistan+ spectrum loading.

In an effort to understand why the FASTRAN life predictions on the Cold-Turbistan+ spectrum tests fell very short, the predicted crack-opening-load ratios are presented in Figure 2.14. The normalized load against time for a small portion of the spectra is compared with the calculated crack-opening-load ratios. The results are somewhat surprising, in that, the calculated crack-opening loads are generally at the minimum load values for the larger cyclic amplitudes. This would imply that the loading cycle would be fully effective in growing the crack, which may be the reason for the shorter predicted fatigue lives. From the early development of the FASTRAN code, the compressive constraint factor (β) had been set to unity, which may cause the material around the crack-tip region to yield more in compression. Thus, a study on the

compressive constraint factor using three-dimensional elastic-plastic finite-element analyses would be extremely useful. In addition, there could always be an error in the code under spectrum loading, which may be causing the crack to grow faster. This will require further study.

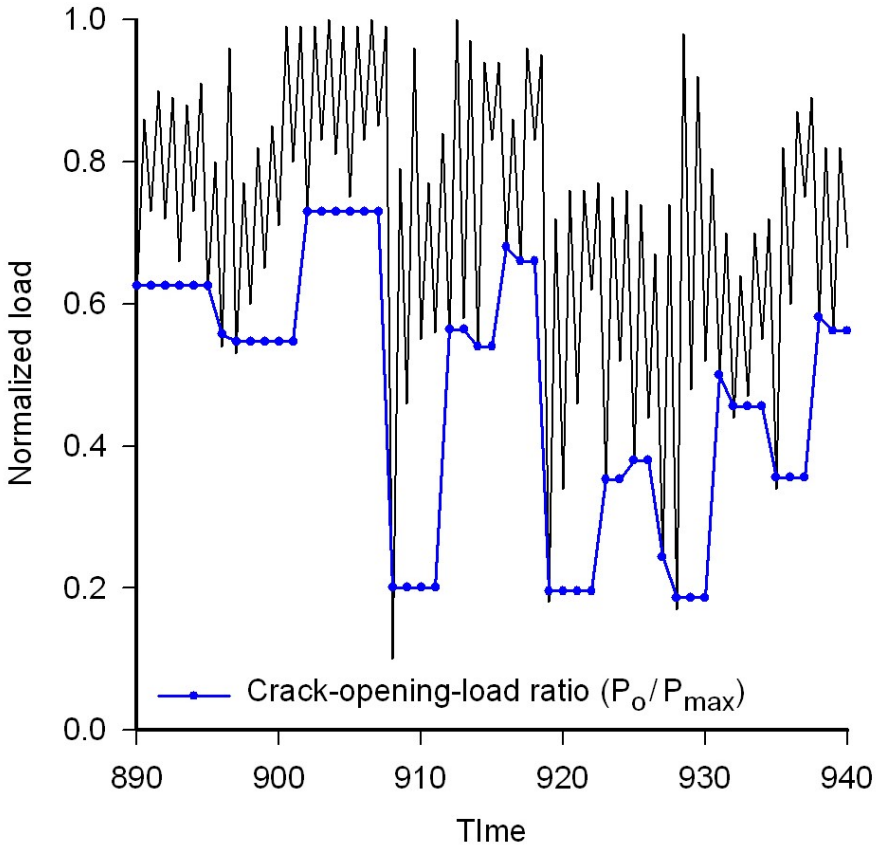

Figure 2.14 Calculated crack-opening-load ratios for part of Cold-Turbistan+ spectrum loading.

Figure 2.15 shows a comparison between the crack-closure model and linear-cumulative-damage (LCD) life prediction for the Cold-Turbistan+ spectrum. LCD assumes that each cycle (only the loading portion) is under constant-amplitude loading

with the steady-state crack-opening loads from the closed form equation [31]. The results from the LCD predictions agreed better with the test data.

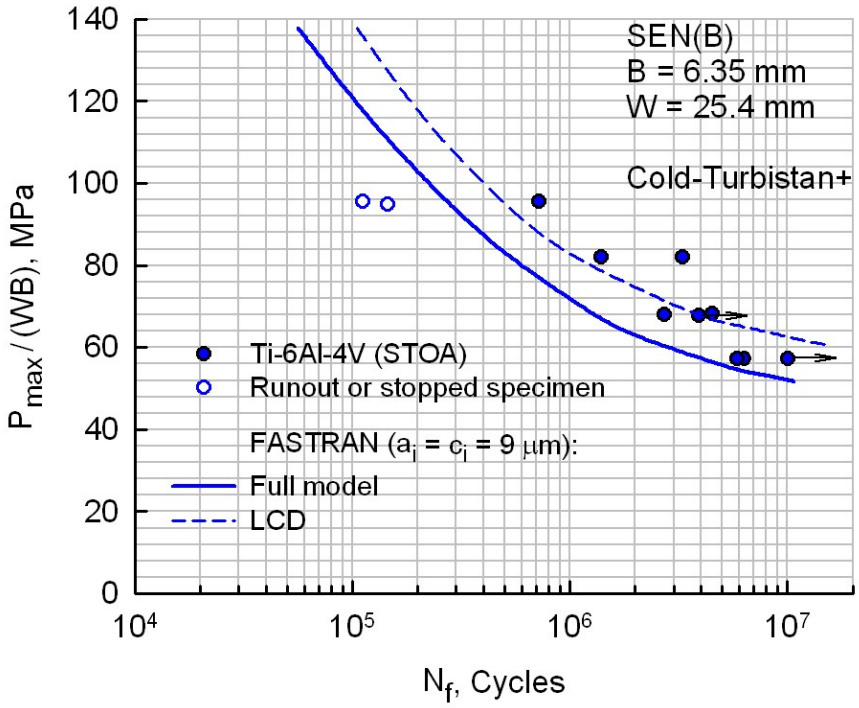

Figure 2.15 Fatigue life predictions from FASTRAN under Cold-Turbistan+ spectrum loading using full model and LCD.

2.9. Concluding Remarks

Titanium alloy (Ti-6Al-4V) plates were provided by the University of Dayton Research Institute (UDRI), which were remnants from a United States Air Force High-Cycle-Fatigue program, that were in the solution treated and over-aged (STOA) condition and produced in accordance with AMS 4928. Single-edge-notch-bend, SEN(B), fatigue specimens were machined from the plates. These specimens were tested under two

constant-amplitude load ratios (R = 0.1 and 0.5) and a Cold-Turbistan+ engine spectrum. All of the tests were conducted under laboratory air and room temperature conditions.

Fatigue-crack-growth-rate data on compact, C(T), specimens machined from the same titanium alloy (Ti-6Al-4V STOA) plate had previously been tested at Mississippi State University, and the test data were used to generate the closure-based effective stress-intensity factor against rate relation. Calculated fatigue lives from FASTRAN using small-crack theory with an equivalent-initial-flaw-size (semi-circular surface flaw at center of notch) of 9 μm in radius was found to fit the constant-amplitude test data at R = 0.1 very well. Then the same initial flaw size was used to predict the constant-amplitude results under R = 0.5 loading. Again, the predicted results at the high-R conditions agreed very well with the test data. Fatigue scatter at the two constant-amplitude loading conditions were also modeled well with a 5 μm and 18 μm radius flaw. However, the FASTRAN analyses underpredicted the Cold-Turbistan+ spectrum loading results by about a factor of 2 to 3. Reasons for the large underprediction were discussed. Life predictions made with linear-cumulative damage (LCD) calculations with the 9 μm initial flaw agreed fairly well on the spectrum tests.

Sustained incremental advances made in stress-intensity factors, plasticity-induced crack closure, constraint effects on crack-tip plasticity, small-crack theory, and understanding load-history effects in the low-rate (threshold) regime have enabled modern Fracture Mechanics to help realize the vision established by Paul Paris and Bill Anderson over a half-century ago.

2.10. References

[1] Paris, P. C., Gomez, M. and Anderson, W. E. (1961) A Rational Analytic Theory of Fatigue. *The Trends in Engineering*, 13, 9-14.

[2] Griffith, A.A. (1920) The Phenomena of Rupture and Flow in Solids. *Philosophical Transactions, Series A,* 221, 163-198.

[3] Irwin, G. R. (1957) Analysis of Stresses and Strains near the End of a Crack Traversing a Plate. *Journal of Applied Mechanics*, 24, 361-364.

[4] Irwin, G. R. (1962) Crack-Extension Force for a Part-Through Crack in a Plate. *Journal of Applied Mechanics*, 29(4), 651-654.

[5] Raju, I. S. and Newman, J. C., Jr. (1979) Stress-Intensity Factors for a Wide Range of Semi-Elliptical Surface Cracks in Finite-Thickness Plates. *Engineering Fracture Mechanics*, 11(4), 817-829.

[6] Newman, J. C., Jr. and Raju, I. S. (1986) Stress-Intensity Factor Equations for Cracks in Three-Dimensional Finite Bodies Subjected to Tension and Bending Loads. *Computational Methods in the Mechanics of Fracture*, S. N. Atluri, ed., Elsevier, pp. 311-334.

[7] Elber, W. (1970) Fatigue Crack Closure under Cyclic Tension. *Engineering Fracture Mechanics*, 2(1), 37-45.

[8] Elber, W. (1971) The Significance of Fatigue Crack Closure. *ASTM STP 486*, pp. 230-242.

[9] Newman, J. C., Jr. (1981) A Crack Closure Model for Predicting Fatigue Crack Growth under Aircraft Spectrum Loading. *ASTM STP 748*, American Society for Testing and Materials, Philadelphia, PA, 53-84. (Also NASA TM-81941, January 1981)

[10] Irwin, G. R. (1960) Plastic Zone near a Crack and Fracture Toughness. Proceedings 7th Sagamore Conference, pp. IV-63-78.

[11] Newman, J. C., Jr. (1992) Fracture Mechanics Parameters for Small Fatigue Cracks. Small-Crack Test Methods, *ASTM STP-1149*, J. Larsen and J. E. Allison, eds., 6-33.

[12] Newman, J. C., Jr. (1992) Effects of Constraint on Crack Growth under Aircraft Spectrum Loading. Fatigue of Aircraft Materials, Eds: A. Beukers, T. deJong, J. Sinke, A. Vlot and L. B. Vogelesang, 83-109.

[13] Newman, J. C., Jr., Crews, J. H., Jr., Bigelow, C. A. and Dawicke, D. S. (1995) Variations of a Global Constraint Factor in Cracked Bodies under Tension and Bending Loads. Constraint Effects in Fracture: Theory and Applications, ASTM STP 1244, M. Kirk and A. Bakker, eds., 21-42.

[14] Pippan, R. (1987) The Growth of Short Cracks under Cyclic Compression. *Fatigue and Fracture of Engineering Materials and Structures Journal*, 9, 319-328.

[15] Newman, J. C., Jr., Schneider, J., Daniel, A. and McKnight, D. (2005) Compression Pre-cracking to Generate Near Threshold Fatigue-Crack-Growth Rates in Two Aluminum Alloys. *International Journal of Fatigue*, 27, 1432-1440.

[16] Newman, J.C., Jr. and Yamada, Y. (2010) Compression Precracking Methods to Generate Near-Threshold Fatigue-Crack-Growth-Rate Data. *International Journal of Fatigue*, 32, 879-885.

[17] Newman, J. C., Jr. (1997) The Merging of Fatigue and Fracture Mechanics Concepts: A Historical Perspective. *ASTM STP-1321*, American Society for Testing and Materials, Philadelphia, PA, 3-54.

[18] Standard Test Method for Measurement of Fatigue Crack Growth Rates (2012) *ASTM E-647*, West Conshohocken, PA.

[19] Hudak, S., Jr., Saxena, S., Bucci, R. and Malcolm, R. (1978) Development of Standard Methods of Testing and Analyzing Fatigue Crack Growth Rate Data – Final Report. AFML TR 78-40, Materials Laboratory, WPAFB, OH.

[20] Gallagher, J. P. (2001) Improved High-Cycle Fatigue (HCF] Life Prediction. AFRL-ML-WP-TR-2001-4159.

[21] Newman, J.C., Jr., Ruschau, J.J., and Hill, M.R. (2011) Improved Test Method for Very Low Fatigue-Crack-Growth-Rate Data. *Fatigue and Fracture Engineering Materials and Structures*, Vol. 34, No. 4, 270-279.

[22] Ruschau, J.J. and Newman, J.C., Jr. (2008) Compression Precracking to Generate Near Threshold Fatigue Crack Growth Rates in an Aluminum and Titanium Alloy. *Journal of ASTM International*, Vol. 5, No. 7, www.astm.org.

[23] Newman, J. C., Jr., Yamada, Y., Ziegler, B. M. and Shaw, J. W. (2014) Small- and Large-Crack Databases for Rotorcraft Materials. DOT/FAA/TC-13/29.

[24] Newman, J. C., Jr., and Edwards, P. R. (1988) Short-Crack Growth Behaviour in an Aluminum Alloy - an AGARD Cooperative Test Programme. AGARD R-732.

[25] ten Have, A. A. (1987) Cold Turbistan - Final Definition of a Standardized Fatigue Test Loading Sequence for Tactical Aircraft Cold Section Engine Disc. Nationaal Lucht-en Ruimtevaartlaboratorium, NLR TR 87054 L.

[26] Donald, J. K. and Blair, A. (2009). Automated Fatigue Crack Growth Testing and Analysis – Series 2001. Version 3.09, Fracture Technology Associates, LLC, Bethlehem, PA.

[27] Dugdale, D. S. (1960) Yielding of Steel Sheets Containing Slits, Journal of Mechanics and Physics of Solids," Vol. 8, No.2, 1960, pp. 100-104.

[28] Newman, J. C., Jr., "A Nonlinear Fracture Mechanics Approach to the Growth of Small Cracks," AGARD CP-328, 1983, pp. 6.1-6.26.

[29] McClung, R. C., "Finite-Element Analysis of Specimen Geometry Effects on Fatigue Crack Closure," Fatigue and Fracture of Engineering Materials and Structures, Vol. 17, 1994, pp. 861-872.

[30] Tada, H., Paris, P. C. and Irwin, G. R. (2000) The Stress Analysis of Cracks Handbook, ASME Press.

[31] Newman, J. C., Jr. (2013) FASTRAN—A Fatigue Crack Growth Life Prediction Code Based on the Crack-Closure Concept. Version 5.4 User Guide. Fatigue and Fracture Associates, LLC, Eupora, MS.

[32] Newman, J. C., Jr. (1984) A Crack Opening Stress Equation for Fatigue Crack Growth. *International Journal of Fracture*, Vol. 24, R131-Rl35.

[33] Garr, K. R. and Hresko, G. C. (2000) A Size Effect on the Fatigue Crack Growth Rate Threshold of Alloy 718. *ASTM STP 1372*, American Society for Testing and Materials, W. Conshohocken, PA, 155-174.

[34] Sonsino, C. M. (2007) Course of SN-Curves Especially in the High-Cycle Fatigue Regime with Regard to Component Design and Safety. *International Journal of Fatigue*, Vol. 29, No. 12, 2246-2258.

[35] Newman, J. C., Jr. (2015) Fatigue and Crack Growth Analyses under Giga-Cycle Loading on Aluminum Alloys. *Procedia Engineering*, Prague, Czech Republic, Elsevier Ltd., Vol. 101, 339-346.

[36] Newman, J. C., Jr. (1973) Fracture Analysis of Surface- and Through-Cracked Sheets and Plates. *Engineering Fracture Mechanics*, Vol. 5, No. 3, 667-689.

[37] Newman, J. C., Jr. and Raju, I. S. (1985) Prediction of Fatigue Crack-Growth Patterns and Lives in Three-Dimensional Cracked Bodies, Advances in Fracture Research, *Proceedings of the 6th International Conference on Fracture*. (Also NASA TM-85787, 1984)

CHAPTER III

CONCLUSIONS AND FUTURE WORK

3.1. Conclusions

Titanium alloy solution treated and over-aged (Ti-6Al-4V STOA) plates were provided by the University of Dayton Research Institute, which were remnants from a United States Air Force High-Cycle-Fatigue program. Single-edge-notch-bend, SEN(B), specimens were machined from the plates. Fatigue tests were performed on the single-edge-notch-bend, SEN(B), specimens under two constant amplitude stress ratios (R = 0.1 and 0.5) and a modified Cold-Turbistan+ engine spectrum loading under laboratory air and room temperature conditions. Predicted fatigue lives from FASTRAN using small-crack theory with an equivalent-initial-flaw-size (semi-circular surface flaw at the center of notch) of 9 μm in radius was found to fit the constant-amplitude test data at R = 0.1 very well. Then the same initial flaw size was used to predict the constant-amplitude results under R = 0.5 loading. Again, the predicted results at the high-R conditions agreed very well with the test data. Fatigue scatter at the two constant-amplitude loading conditions were also modeled well with a 5 μm and 18 μm radius flaw. However, the FASTRAN analyses underpredicted the Cold-Turbistan+ spectrum loading results by about a factor of 2 to 3. Reasons for the large underprediction were discussed. Life predictions made with linear-cumulative damage (LCD) calculations with the 9 μm initial flaw agreed fairly well on the spectrum tests. In observing the fatigue surfaces with the

naked eye, some dark features were found along the notch root that may have indicated the nucleation site(s). Both optical and scanning-electron-microscope (SEM) analyses were made try to identify some of these features. The SEM analysis shows some features that look like the fatigue failures came from micro-machining marks and not the material micro-structure. The depth of the machining mark was about 7.4 μm, and the possible depth of the feature was about 14.8 μm. The EIFS of 9 μm was remarkably close to this micro-machining feature.

3.2.Future Work

Further efforts are required to develop a test procedure to generate extremely low crack-growth rates below 1.0e-10 m/cycle. In such regimes, crack growth is not a cycle-by-cycle basis, but intermittent, where crack fronts may stop at grain boundaries or other microstructural features and take many cycles to re-initiate. Advanced measurement and pattern recognition procedures may have to be developed using a scanning-electron-microscope on small surface- and corner-crack propagation. Further study needs to be performed on the compressive constraint factor (β) using three-dimensional elastic-plastic finite element analyses for advancement of fatigue-life prediction code, like FASTRAN.